frontiers | Frontiers in Earth Science

TYPE Original Research
PUBLISHED 10 January 2023
DOI 10.3389/feart.2022.933031

OPEN ACCESS

EDITED BY
Ya Ping Wang,
East China Normal University, China

REVIEWED BY
Kiichiro Kawamura,
Yamaguchi University, Japan
Davide Tiranti,
Agenzia Regionale per la Protezione Ambientale del Piemonte (Arpa Piemonte), Italy

*CORRESPONDENCE
Hongxian Shan,
hongxian@ouc.edu.cn
Yonggang Jia,
yonggang@ouc.edu.cn

SPECIALTY SECTION
This article was submitted to Geohazards and Georisks, a section of the journal Frontiers in Earth Science

RECEIVED 30 April 2022
ACCEPTED 23 September 2022
PUBLISHED 10 January 2023

CITATION
Xue L, Liu H, Li Z, Sun Z, Shan H and Jia Y (2023), In situ observation of wave-induced deformation of submarine landslides in tidal channel areas. *Front. Earth Sci.* 10:933031. doi: 10.3389/feart.2022.933031

In situ observation of wave-induced deformation of submarine landslides in tidal channel areas

Liang Xue[1,2], Hanlu Liu[1,2], Zhenghui Li[1,2], Zhongqiang Sun[1,2], Hongxian Shan[1,2,3]* and Yonggang Jia[1,2,3]

[1]Shandong Provincial Key Laboratory of Marine Environment and Geological Engineering, Ocean University of China, Qingdao, China, [2]Laboratory for Marine Geology, Qingdao National Laboratory for Marine Science and Technology, Qingdao, China, [3]Key Laboratory of Marine Environment and Ecology, Ministry of Education, Ocean University of China, Qingdao, China

Landslides often occur in land slopes, estuaries, fjords, and intertidal zones in the marine environment, while landslides in tidal channels have not been systematically reported. The Zhoushan sea area is dotted with islands and crisscross tidal channels, which is a typical tidal channel development area. The data from the coastal zone and island survey, offshore engineering site selection, and environmental survey show that landslides are very common in tidal channel areas. The detailed study of this kind of landslide will enrich the research theory of submarine landslide and have important guiding significance for marine planning, development and site selection, and construction of coastal engineering in coastal areas. First, the submarine landslide in southwest of Zhujiajian Island in Zhoushan is investigated in this study. It is found that the sliding zone is parallel to the island coastline, with a length of about 250 m and an extension of 2 km, and the buried depth of the sliding surface is generally 8–10 m; then, through the self-developed seabed deformation observation system, combined with the hydrodynamic observation system, the landslide was observed *in situ* for 75 days. The observation results showed that the landslide slides at a constant speed along the sliding surface under the action of weight; the slides accelerate under the action of waves, and multiple sliding surfaces are generated in the landslide body at the same time. Finally, the genetic mechanism of submarine landslides in tidal channel areas is put forward.

KEYWORDS

submarine landslide, *in situ* observation, storm wave, seabed creep deformation, multistage sliding

Introduction

Marine resources are an important part of natural resources. The rational development of marine resources is related to the sustainable development of human society in the future. There are many kinds of marine geological disasters, and the laws of disaster occurrence and development are complex and difficult to predict (Liu et al., 2020). With the rapid development of science and technology in recent years, especially the continuous emergence of modern remote sensing technology, wireless communication technology, and various sensing technologies, the early identification, monitoring, and early warning of hidden dangers of geological disasters have become an important means of active prevention and control of geological disasters (Xu, 2020).

Seabed instability will lead to submarine landslide, collapse depression, and other geological disasters. Some scholars have proposed various seabed deformation and sliding modes such as translational, rotational, and slump based on the geophysical survey, indoor test, and other research methods (Xu, 2006; Yang and Chen, 1994; Chang, 2009), which pose a serious threat to the safety of submarine pipelines, platforms, and other engineering structures. The real mechanism of instability triggering of the *in situ* submarine slope is not caused by a single factor but more by very complex mutual coupling in different periods (Prior, 1986a; Yang and Chen, 1994; Wang, 2015). During the cyclic action of ocean dynamics (waves, tides, etc.) on the seabed, it will exert vertical pressure, tension, and horizontal shear force on sediments. Under the action of this cyclic load, pore water pressure accumulates in the sediment, and the strength of the sediment decreases. When the strength is not enough to resist the force of ocean power, the sediment will deform and slide at different scales, which may further lead to large-scale submarine landslides and harm to marine engineering (Sultan et al., 2007; Liu et al., 2015; Liu et al., 2016; Nian et al., 2016).

At present, the investigation and research of submarine landslides mainly rely on marine geophysical detection technologies such as side scan sonar and shallow formation profile technology. The occurrence process and triggering factors of landslides can only be known by speculation (Vanneste et al., 2014; Jia et al., 2017). In contrast, seabed *in situ* observation technology can obtain dynamic observation data with timeliness, which is more conducive to the study of the occurrence mechanism and evolution process of submarine landslides (Zhang et al., 2016). Prior and others used sediment dynamic observation devices to record acceleration and inclination changes and found the revival of submarine landslide induced by storm surge in the underwater delta of the Yellow River (Prior et al., 1989); Chadwick et al. (2012) and Wallace et al. (2016) used high-precision water pressure gauges to monitor seabed subsidence and uplift in the deep sea so as to predict the time of volcanic eruption and capture the process of tectonic movement; Blum et al. (2010) used the seabed acoustic measurement system to monitor the unstable slope of the seabed for the first time; Urlaub et al. (2018) used the acoustic measurement system and pressure gauge to capture the sliding deformation process of the flank of Etna volcano; and Wang successfully captured the seabed deformation process induced by storm surge in the underwater delta of the Yellow River using the submarine landslide monitoring system (SLM) and put forward the mechanism of wave induced seabed instability in the underwater delta of the Yellow River (Wang et al., 2018; Wang et al., 2020).

The Zhoushan archipelago is located in the northeast of Zhejiang Province. It is composed of more than 1,300 islands of different sizes. It is the largest archipelago in China and rich in fishery resources, with many deep-water ports and developed shipping channels. It is a key logistic transit base in the Yangtze River Delta and its surrounding areas and has an important strategic position. Submarine landslides of different sizes are widely developed in the Zhoushan sea area. Among them, there are many gorge tidal channels in the south of Zhoushan Islands. A large number of submarine landslides are developed in these channels. The vast majority of landslides are an overall failure, mainly slicing and sliding along the slope. Ye et al. (1996), Lai et al. (2000), and Lai and Ye (2011) concluded that the uneven distribution of erosion and deposition in the tidal channel leads to the continuous increase of the seabed slope, and finally, the overall sliding failure occurs under the action of gravity as the main driving force. Marine geological disasters represented by submarine landslides pose a great threat to the safety of offshore engineering facilities in the Zhoushan sea area. It is particularly important to explore the excitation mechanism and cause mechanism of submarine deformation disasters such as submarine landslides.

Based on the self-developed *in situ* observation system, this study carried out *in situ* observation for 75 days on the typically inclined seabed slope in the southwest of Zhujiajian Island, Zhoushan, and obtained the observation data of lateral deformation and deformation direction of sliding surface (Xue et al., 2020; Liang et al., 2021).

The Zhoushan archipelago is located in the south of the Yangtze River Estuary. As the largest estuary in China, a large amount of sediment carried by the Yangtze River is deposited near the Zhoushan archipelago during its southward migration. Therefore, this area is a typical distribution area of muddy coast. After preliminary field exploration, the sea area in the southwest of Zhujiajian Island is selected as the *in situ* long-term observation area. Zhujiajian Island is located in the southeast of the Zhoushan archipelago in Zhejiang Province, with a maximum length of 13 km in the North-South direction and 7 km in the East-West direction. It is the fifth largest island in the Zhoushan archipelago (Feng, 2012). The observation area is the submarine landslide area in the southwest of Zhujiajian Island in the Zhoushan archipelago (Figure 1A), which is located on the northeast slope of the tidal scouring trough and close to the

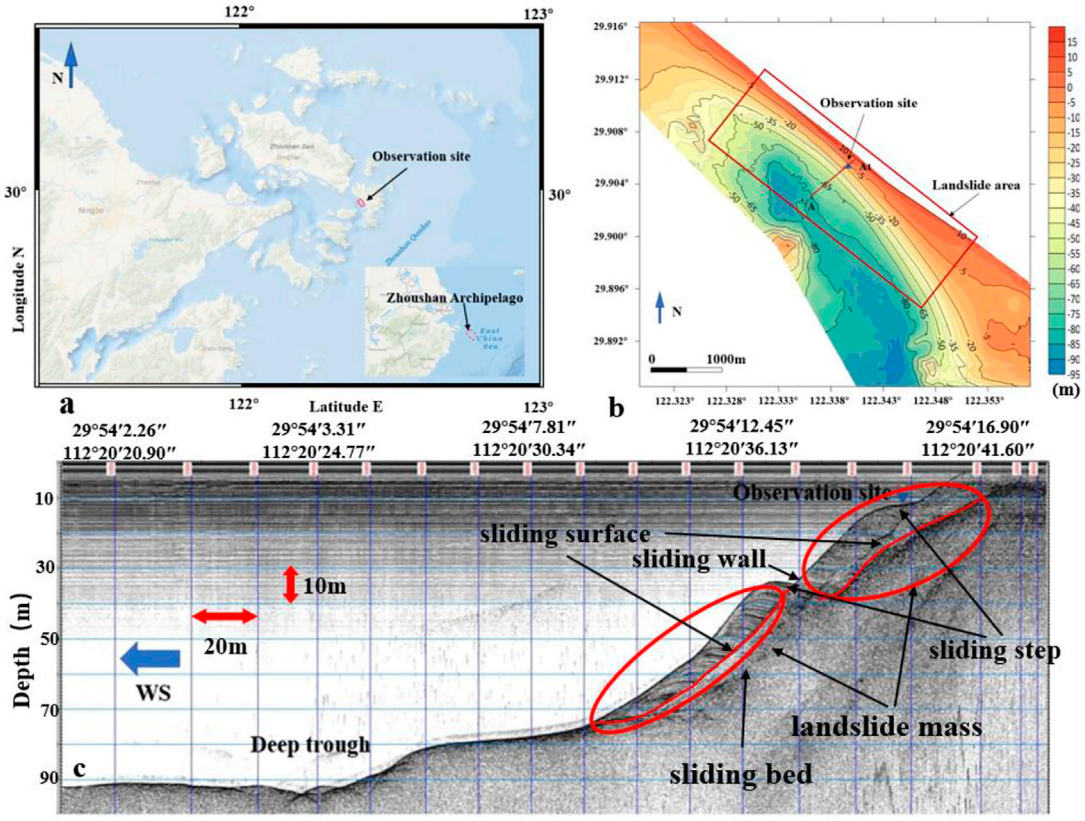

FIGURE 1
Geographical location map, water depth topographic map, and shallow stratum profile of the study area. **(A)** Shows the map of the Zhoushan archipelago, China, with the Zhujiajian study area marked with a red rectangle. **(B)** Shows the multibeam topographic map of study area with the observation site highlighted within the blue triangle. **(C)** Shows subbottom profiling of a scarp near the observation site denoted by a blue triangle.

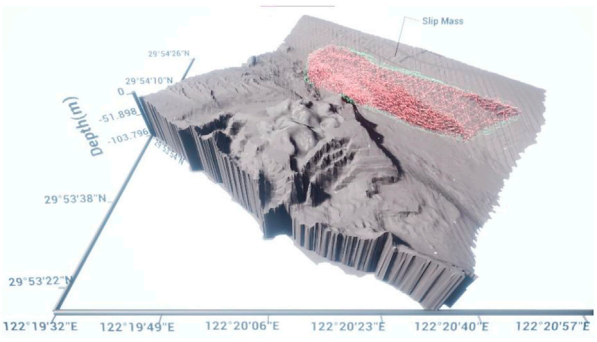

FIGURE 2
Schematic diagram of the Zhujiajian landslide.

Fulimen reclamation project of Zhujiajian Island. This area belongs to a typical tidal channel development area, with tidal channels crisscrossing and many landslides occurring (Liu et al., 2007). The tidal category of the observed sea area is the regular semidiurnal tide. The velocity of a rising tide is significantly faster than that of a falling tide, with an average tidal range of 2.5–2.8 m and a maximum tidal range of 4.79 m. Waves are mainly wind waves, and big waves are mostly caused by windy weather. The annual average wave height is 0.1 m, and the regular wave is southward (Chen et al., 1982; Zhang, 2013).

The water depth of the observation points selected in this study is about 10–12 m. The local terrain is flat, and the slope is small. There are steep slopes in the southwest, with an average slope of 8–9°, as shown in Figure 1B. Clear landslide mass, sliding surface, sliding bed, sliding wall, and sliding step can be seen from the records of the shallow stratum section. Irregular "feathery" bedding can be seen in the sliding body with the structural characteristics of a traction landslide (Figure 1C).

The boundary and shape of landslide mass in combination with multi-beam and shallow section data were drawn (Figure 2). The whole sliding zone is parallel to the island coastline, extending about 2 km and about 250 m in length. The water depth extends from about 5 m near the shore to about 70 m. The

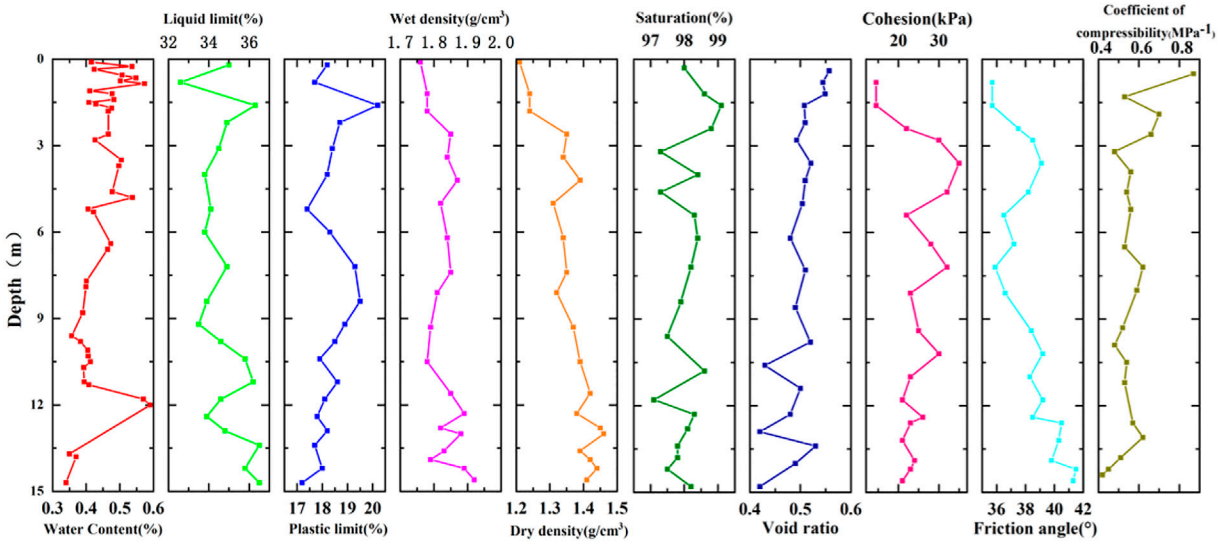

FIGURE 3
Physical and mechanical properties of seabed soils at a depth of 15 m.

buried depth of the sliding surface is generally 5–6 m, up to about 15 m.

A 15-m core sample extracted from the observation site showed mainly gray muddy clay and silty clay, with mud–sand interbedding, whose silt content >70% (Figure 3).

Materials and methods

Monitoring equipment

Seabed deformation and sliding are the most intuitive indices to reflect seabed stability. On the one hand, the observation data can help us analyze the deformation characteristics of preseabed geological disasters and provide strong evidence for the study of disaster mechanisms. On the other hand, they can provide early warning for marine engineering and ensure the safety of engineering and personnel. At home and abroad, most of the investigation and research on the deformation process of seabed sediments are geophysical investigation, sediment sampling, model test, numerical calculation, and other methods; therefore, it is difficult to obtain the field dynamic data of the deformation process of seabed sediments. Due to the complex engineering and dynamic geological process of the seabed, the implementation of *in situ* observation is difficult and the technical requirements for observation equipment are high. Therefore, the research on the deformation and sliding process of the seabed, especially the *in situ* observation method of the large-scale long-distance sliding migration process, is in the exploratory stage at home and abroad.

The *in situ* observation system of shallow water sediment deformation process applied in this paper consists of a deformation observation system and a supporting observation system. The deformation observation system is built with the array displacement meter as the core, which can realize the *in situ* real-time observation of the vertical deformation of seabed sediments and the lateral deformation process at different depths. The data acquisition and storage system can collect and store the lateral and vertical deformation data of seabed sediments obtained by the deformation observation system. The power supply system is composed of a high-capacity lithium battery pack and an underwater sealed cabin, which can provide long-term power supply for the deformation observation system and data transmission system. The supporting observation system is composed of a hydrodynamic condition observation system, which can carry out *in situ* long-term observation of marine dynamic conditions and seabed sediment deformation process at observation points at the same time so as to provide more comprehensive and timely data support for the analysis and discussion of the sediment deformation process.

The *in situ* seabed deformation observation system is composed of an array displacement meter, data acquisition, a storage system, and a power supply system (Figure 4A). The core component of deformation observation is the array displacement meter, which is composed of multiple rigid measurement units of equal lengths. The measurement units are connected in parallel, which can bend in any direction but resist torsional movement (Figure 4B). A high-precision MEMS accelerometer is integrated into the measurement unit to obtain the bending angle and

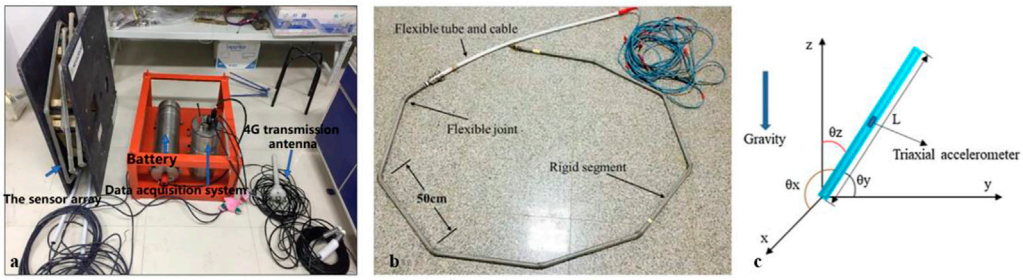

FIGURE 4
Seabed deformation observation system and working principle. **(A)** Shows the physical map of the seabed deformation observation system, **(B)** shows the physical map of sensor array, and **(C)** shows the sketch map of the single shape accel array segment.

direction of each observation node by sensing the change of acceleration field and then calculate the deformation of each observation unit by relying on the built-in microprocessor (Figure 4C). The rigid rods of array displacement sensors are connected together through nodes so that the *X*, *Y*, and *Z* coordinate systems of adjacent rods are associated so as to accumulate the spatial coordinate positions of each node point (Danisch et al., 2007). This method is based on the principle that the three-dimensional shape sensing system is constrained by degrees of freedom along the path and was originally applied to the optical fiber curvature sensor (Danisch et al., 1999). The calculation of the deformation of the array displacement sensor is divided into two steps. First, the original data is converted into triaxial acceleration (a triaxial component of gravity acceleration), and then a 3D displacement calculation is carried out.

The first step of the calculation is to analyze how the triaxial acceleration of each rod section is distributed in the gravity field to determine the initial space attitude of each segment in the static state. The relationship between angle and spatial attitude is calibrated by the array displacement sensor manufacturer before leaving the factory. The length of each segment is known (L = 50 cm); therefore, we can determine the coordinate value of the tail node of each rod segment ($L\cos\theta_x, L\cos\theta_y, L\cos\theta_z$). For the array displacement sensor of the whole multi-rod section, the coordinate value of the tail end of each rod section is calculated by accumulating the coordinate value of the previous rod section one by one ($\sum_{k=1}^{n} L\cos\theta_{xn}$; $\sum_{k=1}^{n} L\cos\theta_{yn}$; $\sum_{k=1}^{n} L\cos\theta_{zn}$). When the array displacement sensor deforms, the spatial attitude of each rod section will change. The displacement change of each node of the array displacement sensor can be obtained by calculating the difference between the corresponding coordinate value at this time and the initial coordinate value.

Taking the displacement change of each axis in section *n* as an example, the calculation formula is as follows:

$$\begin{aligned}\Delta x &= \sum_{k=1}^{n} L\cos\theta_{xnt_1} - \sum_{k=1}^{n} L\cos\theta_{xnt_0}\\ \Delta y &= \sum_{k=1}^{n} L\cos\theta_{ynt_1} - \sum_{k=1}^{n} L\cos\theta_{ynt_0}\\ \Delta z &= \sum_{k=1}^{n} L\cos\theta_{znt_1} - \sum_{k=1}^{n} L\cos\theta_{znt_0}\end{aligned} \quad (1)$$

where t_1 and t_0 represent the measurement cutoff time and the initial time, respectively, and the calculation results represent the displacement change of each axis between the two times.

In order to ensure the accuracy of the measurement, the first-rod segment (i.e., reference point) must be stationary. When the array displacement sensor is placed vertically in the seabed, the calculation is simplified by ignoring the coordinate value of the *Z*-axis, which is almost unchanged during horizontal deformation.

Since the calculation is gradually accumulated through the first-rod section, the corresponding error will also accumulate with the increase of the length of the array displacement sensor. The measurement accuracy of the sensor is 0.5 mm/32 m. The shorter the length, the higher the accuracy. The calculation formula is as follows:

$$\varepsilon = \sqrt{\frac{X}{32}} \cdot 0.5\text{mm} \quad (2)$$

where ε is the measurement error of the sensor and X is the distance from the node to the origin (fixed point).

Array displacement meter has the advantages of high precision, large range, high stability, and reusability and has achieved good results in the application of monitoring and early warning of landslides on land (Chen et al., 2015; Wei, 2015; Uhlemann et al., 2016).

Equipment emplacement

In this study, the array displacement sensor is vertically placed in the *in situ* seabed sediment, and the deformation of the sediment is quantified by the deformation of the sensor. The

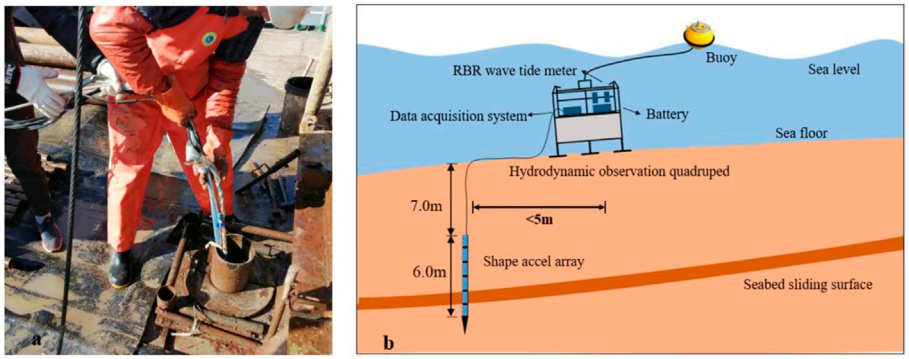

FIGURE 5
(A) Offshore drilling used to emplace the shape accel array. **(B)** Emplacement setup of the submarine landslide observation system, including the position of the shape accel array and hydrodynamic observation quadruped.

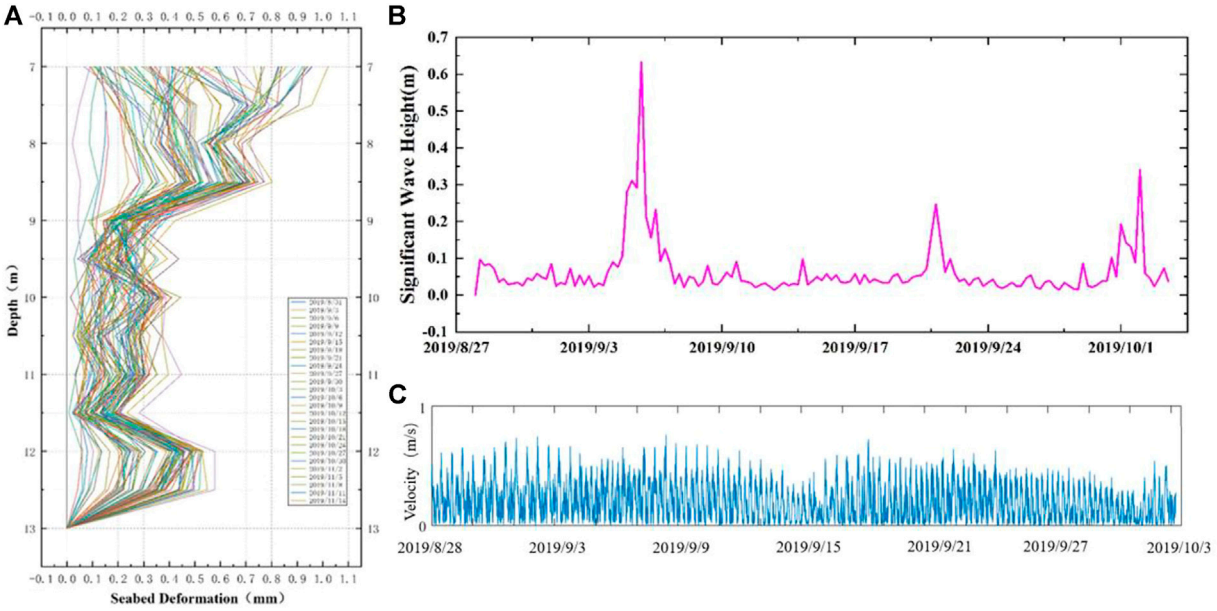

FIGURE 6
(A) Time series of cumulative horizontal deformation of the shape accel array, attached with the significant wave height **(B)** and the flow rate **(C)**.

French Institute for Marine Development (INFREMER) made the first attempt at its deployment method (Stegmann et al., 2012). The inclinometer probe developed by INFREMER is also composed of an array displacement sensor, and the layout method is a free-fall gravity penetration. The equipment is used for long-term *in situ* observation on the underwater slope of Nice, France. The landslide surface of the Zhujiajian sea area in the study area of *in situ* observation in this study is relatively deep and cannot penetrate to the specified depth; therefore, its layout method is not suitable. Therefore, in this study, the offshore drilling technology is used to implement the 13-m deep drilling, and the array displacement sensor is vertically buried on the seabed to make the sensor pass through the landslide surface with a fixed counterweight at the bottom making it relatively stationary during observation (Figure 5A). During the placement of the array displacement sensor, the casing pipe is placed while drilling to prevent the hole from collapsing. After the sensor is vertically placed in the hole, the fine sand is backfilled to maintain the vertical attitude of the sensor. At the same time, the rapid settlement of the fine

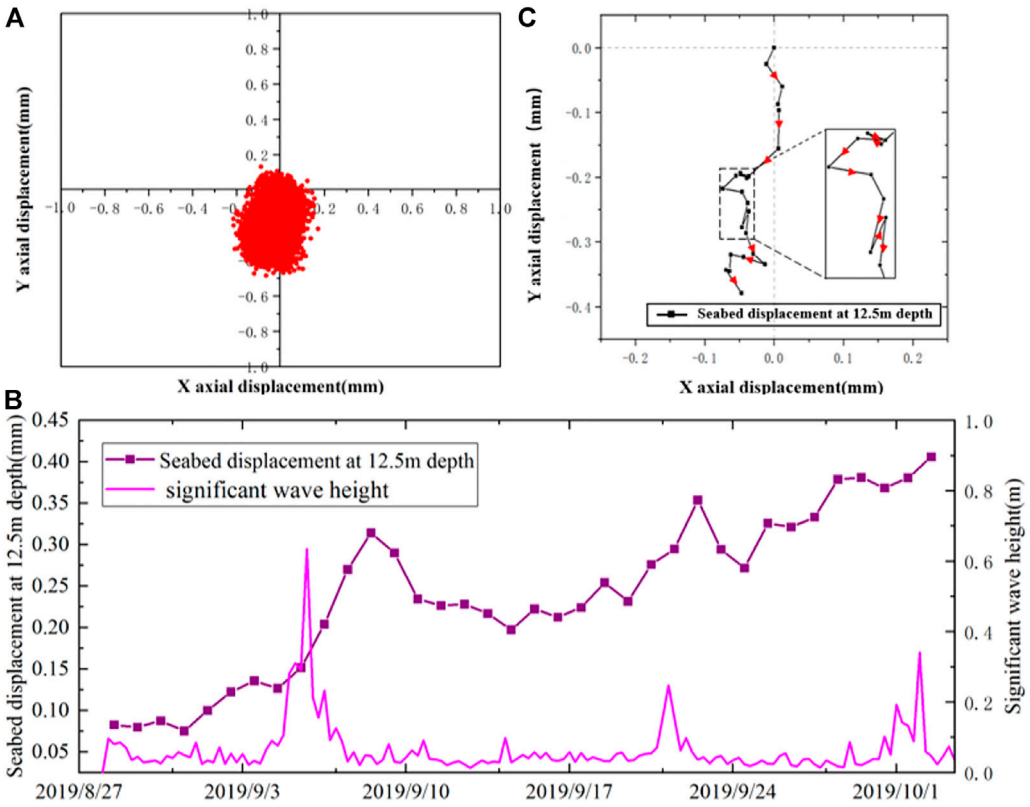

FIGURE 7
(A) Node location during observation at the depth of 12.5 m, **(B)** seabed displacement at 12.5 m depth and significant wave height during observation, and **(C)** deformation direction during storm event at the depth of 12.5 m.

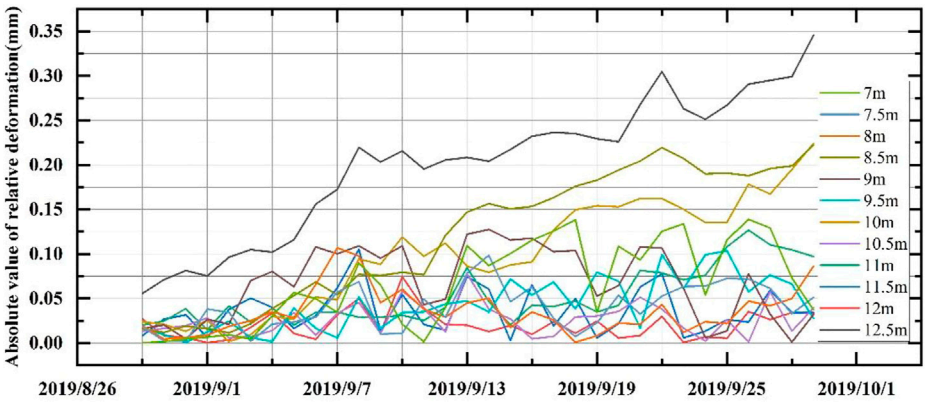

FIGURE 8
Absolute value of relative deformation during observation.

sand will leave the sensor in the hole, and the casing will not be brought out during the recovery process. The placement point of the array displacement sensor is about 5 m away from the quadruped (Figure 5B). The observation system was emplaced in the seabed on 28 August 2019 and recovered on 9 December 2019.

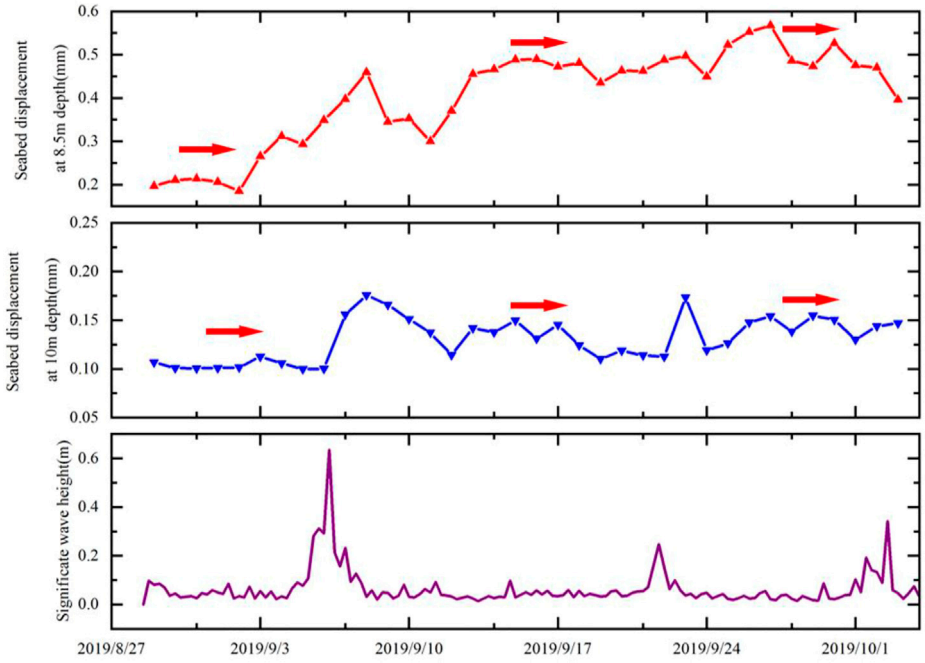

FIGURE 9
Seabed displacement at 8.5 m and 10 m depths and significant wave height during observation.

Observation results

The whole observation is in autumn and winter, during which storms occur frequently. The effective data are selected for analysis and statistics, and the results of *in situ* observation of environmental elements including significant wave height, average current velocity, and seabed deformation are obtained. We conduct statistical analysis on wave data, screen out the abnormal data in the later stage, and conduct statistical analysis with 36 days of low noise and high-quality data. The results show that during the observation period, the maximum deformation of the seabed is 1 mm (Figure 6A), which is greater than the measurement error of the sensor, which can reflect the deformation and sliding of the seabed. During the observation period, the average wave height of the observed sea area was about 0.1 m, during which three obvious storm events were experienced, and the significant wave height increased significantly (6 September with 0.65 m significant wave height; 20 September with 0.3 m significant wave height; 2 October with 0.35 m significant wave height) (Figure 6B). During most of the observation period, the measured velocity of the seabed current is less than 80 cm/s, and the bottom velocity does not change significantly during storm events (Figure 6C).

It can be seen from the aforementioned that the buried depth of the sliding surface of the Zhujiajian landslide is about 12.5 m, and the displacement sensor data at the depth of 12.5 m of the seabed is selected for analysis (Figure 7).

Figure 7A shows the process of the deformation direction at the depth of 12.5 m. The *X*-axis and *Y*-axis represent the two coordinate systems of the array displacement sensor on the horizontal plane, which can be understood as the top view of the sliding surface. The results show that the deformation direction is mainly distributed in the *Y*-axis direction. According to the layout of field equipment, the *Y*-axis direction corresponds to the inclination of the slope, indicating that the deformation direction of the sliding surface is mainly concentrated in the inclination direction.

The external forces causing the deformation and sliding of the seabed slope include the cyclic shear stress generated by the wave load in the sediment, the shear stress formed by the wave current on the seabed surface, and the sliding force caused by the component of gravity along the slope (Jia et al., 2011). Wave current coupling generates bottom flow in the seabed boundary layer, and the bottom shear stress caused is very small, which is only a few pascals even in storm events (Dufois et al., 2008; Wang et al., 2018), and has little effect on the deformation and sliding of sediments in a short time. In addition, no earthquake event occurred near the observation area during the observation period (China Seismic Network Center). The influence of seismic load is not considered in this study. Therefore, the external forces causing the deformation and sliding of seabed slope are mainly gravity and the cyclic shear stress generated by wave load in the sediment.

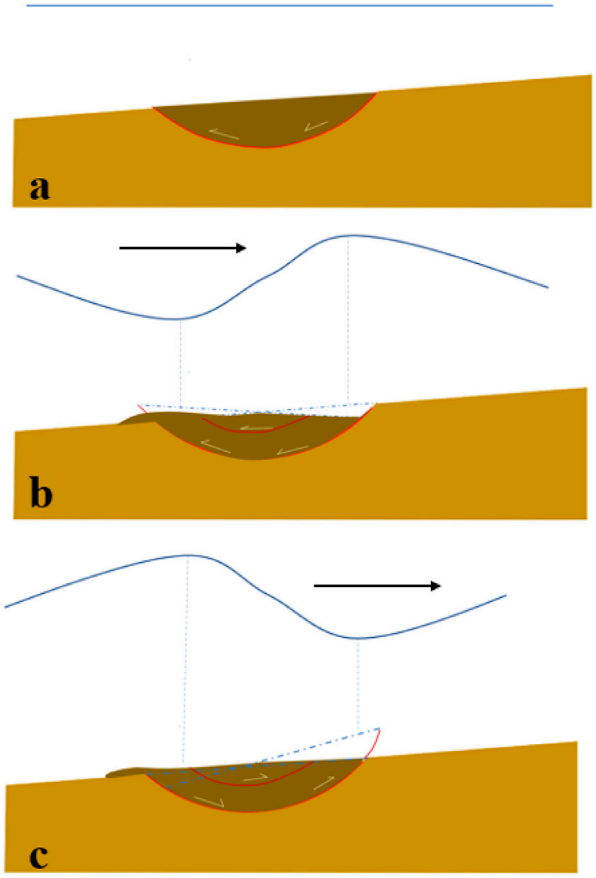

FIGURE 10
Schematic diagram of seabed deformation and sliding in the study area. **(A)** Shows that the seabed slides along the slope of the sliding surface under the action of gravity, **(B)** shows that the direction of shear stress formed by wave crest and wave trough is opposite to the wave direction, and the soil will oscillate clockwise, and **(C)** shows that the direction of shear stress formed by wave crest and wave trough is the same as that of the wave, and the soil will oscillate anticlockwise.

Comparing the deformation data at the sliding surface with the wave data (Figure 7B), it is found that the deformation at the sliding surface gradually increases. Under the calm sea condition, the deformation of the seabed soil at the sliding surface increases slowly, indicating that the landslide is in the limit equilibrium state and slowcreep slide occurs under the action of gravity. During the storm event, significant wave height reached 0.65 m on 6 September, the seabed deformation speed increased, and the same phenomenon occurred in the storm event on 20 September. Due to the hysteretic effect, the deformation slip caused by the storm event on 2 October is not shown. This indicates that the seabed creep slide speed increases under the cyclic shear stress generated by wave load in the seabed and with an obvious hysteretic effect.

The seabed generates horizontal cyclic shear stress under the alternating action of peak compressive stress and trough tensile stress (Liam Finn et al., 1983; de Groot et al., 2006), and cyclic oscillation movement will occur after the seabed sediments become unstable (Liu et al., 2013; Zhang et al., 2018a). According to the *in situ* observation results, the seabed deformation direction is along the negative direction of the *Y* axis, indicating that the seabed deformation is in a gradually progressive process as a whole; during this period, it is accompanied by reciprocating motion, corresponding to the cyclic oscillation deformation of seabed induced by the storm (Figure 7C).

It can be seen from Figure 6A that during the observation process, some nodes at the depth of 7–13 m were found to have larger deformation than adjacent nodes, and there may be some other sliding interfaces. The relative deformation of the sensor at each depth (the absolute opposite value of the deformation difference between the node and the previous node) was processed and analyzed, and the results as shown in Figure 8 were obtained. It was found that except for 12.5 landslide sliding surfaces, there are also obvious sliding interfaces at 8.5 m and 10 m depths. Combined with the borehole data, the corresponding mud–sand interbedding sediment at the depths of 8.5 m and 10 m are found. During the observation, the seabed deformation at 8.5 m and 10 m depths is noted, as shown in Figure 9.

The deformation at 8.5 m and 10 m depths does not change significantly during the observation. During the storm events on 6 September and 22 September, the deformation increased significantly and also had an obvious hysteretic effect; after the storm event, the seabed soil returned to a stable state. This shows that during the storm event, other sliding surfaces will be generated in the landslide mass, and multistage sliding will occur on the slope.

Discussion: Analysis of the submarine landslide deformation pattern

The initiation mechanism of wave-induced sediment instability and further seabed deformation sliding mainly includes liquefaction failure and shear failure (Rahman 1991; Rahman, 1997; Zhang et al., 2016). Simple shear failure is more likely to occur on the seabed of sediments with high clay content, while simple liquefaction failure analysis is mainly aimed at the seabed of cohesionless sediments (Rahman and Jabery 1986; Rahman 1991; Jeng 2001). The soil in the study area is fine, basically belonging to clayey silt or silty clay; therefore, mainly shear failure is seen.

The Zhujiajian landslide has obvious multistage sliding characteristics. In general, the multistage of landslide can be divided into two categories: one is caused by the difference in sliding speed of each part of landslide mass in the first sliding

of soil mass and the other is that a new landslide is generated on the basis of the previous landslide. According to the advancing direction of a landslide, it can be divided into traceability landslide and advancing landslide. The so-called traceable landslide means that the landslide mass has multiple landslides in turn toward the source, and the forward landslide means that the landslide mass follows the direction of the landslide. No matter which type, they all show multilevel step landforms on the section. It can be clearly seen from Figure 1A that two sliding steps can be seen in the main section. The sliding surface along the direction of the landslide is clearer and clearer each time, indicating that the damage develops along the direction of the landslide.

According to the monitoring data, the deformation pattern of the Zhujiajian landslide can be expressed as follows: on the inclined seabed, the slope will creep slide along the landslide tendency under the action of gravity to form an integral circular arc sliding (Figure 10A); under the action of waves, the wave crest and trough form shear stress on the seabed. With the alternating action of wave crest and trough, the seabed soil moves cyclically and the creep slide speed is accelerated. At the same time, there will also be a sliding surface at the position of sediment interbedding in the landslide body, and the soil at the sliding surface also moves cyclically (Figures 10B,C). When the wave action is strong enough, the landslide will have a multistage sliding phenomenon.

Conclusion

Based on the observation system independently developed and designed, this study carried out long-term *in situ* observation on the typically inclined seabed slope in the southwest of Zhujiajian Island, Zhoushan, and obtained hydrodynamic data such as lateral deformation size and direction at different depths of the seabed slope, wave height, and velocity. The following conclusion is obtained.

1. Under the action of weight, Zhujiajian landslide slides slowly and slides along the slope tendency, and the sliding rate is basically unchanged. In storm events, the slope slides accelerate, the sliding rate increases, and the seabed soil moves cyclically with the action of waves; after the storm event, the landslide returned to the original sliding rate.
2. Under calm sea conditions, the landslide is in an overall sliding state. During the storm event, a sliding surface is generated at the mud–sand interbedding sediment in the landslide body. After the storm event, the landslide still slides as a whole.

Data availability statement

The original contributions presented in the study are included in the article/supplementary material; further inquiries can be directed to the corresponding author.

Author contributions

LX: conceptualization, methodology, software, investigation, formal analysis, and writing—original draft; HL: data curation and writing—original draft; HS: visualization and investigation; YJ: resources and supervision; ZS: software and validation; and ZL: visualization and writing—review and editing.

Funding

This work was funded by the Key Project of NSFC-Shandong Joint Research Funding POW3C (U1906230), the National Natural Science Foundation of China (41877223), and Key Science and Technology Plan of Power China Huadong Engineering Corporation Limited (KY2018-ZD-01).

Acknowledgments

The authors deeply appreciate the help of Chunsheng Ji, Ziqi Peng, Tianyang Liang, Yankai Hou, and Naili Hu in carrying out the observations. They thank Peng, Miaojun Sun, and Weida Ni of Power China Huadong Engineering Corporation Limited for their support of the project. Comments from reviewers and the editor greatly improved the manuscript and are highly appreciated.

Conflict of interest

The authors declare that the research was conducted in the absence of any commercial or financial relationships that could be construed as a potential conflict of interest.

Publisher's note

References

Blum, J. A., Chadwell, C. D., and Driscoll, N. (2010). Assessing slope stability in the Santa Barbara Basin, California, using seafloor geodesy and CHIRP seismic data [J]. *Geophys. Res. Lett.* 37 (13), 438–454.

Chadwick, W. W., Dziak, R. P., Haxel, J. H., Embley, R. W., and Matsumoto, H. (2012). Submarine landslide triggered by volcanic eruption recorded by *in situ* hydrophone. *Geology* 40 (1), 51–54. doi:10.1130/g32495.1

Chang, F. (2009). *Study on submarine landslide in the Yellow River Estuary under wave action [D]*. Qingdao: Ocean University of China.

Chen, H., Li, Y., and Fang, R. (2015). Research on new technology of landslide deep displacement monitoring and early warning and prediction [J]. *J. rock Mech. Eng.* 34 (S2), 4063–4070.

Chen, H., Yan, Q., and Xiang, L. (1982). Modern coastal sedimentation of Zhujiajian island in Zhoushan [J]. *J. East China Normal Univ. Nat. Sci. Ed. [J]* (02), 77–91.

Danisch, L. A., Englehart, K., and Trivett, A. (1999). Spatially continuous six degree of freedom position and orientation sensor. *Sens. Rev.* 3541 (2), 106–112. doi:10.1108/02602289910266142

Danisch, L. A., Lowery-Simpson, M. S., and Abdoun, T. H. (2007). Shape-acceleration measurement device and method. *U.S. Pat. no.* 7296, 363.

De Groot, M. B., Bolton, M. D., Foray, P., Meijers, P., Palmer, A. C., Sandven, R., et al. (2006). Physics of liquefaction phenomena around marine structures. *J. Waterw. Port. Coast. Ocean. Eng.* 132 (4), 227–243. doi:10.1061/(asce)0733-950x(2006)132:4(227)

Dufois, F., Garreau, P., Hir, P. L., and Forget, P. (2008). Wave- and current-induced bottom shear stress distribution in the Gulf of Lions. *Cont. Shelf Res.* 28 (15), 1920–1934. doi:10.1016/j.csr.2008.03.028

Feng, S. (2012). *Characteristics and numerical simulation of tidal current and suspended sediment in winter in luotou waterway*. Hangzhou: Zhoushan [D] Zhejiang University.

Jeng, D. S. (2001). Mechanism of the wave-induced seabed instability in the vicinity of a breakwater: A review. *Ocean. Eng.* 28 (5), 537–570. doi:10.1016/s0029-8018(00)00013-5

Jia, Y., Shan, H., and Yang, X. (2011). *Sediment dynamics and geological hazards in the Yellow River estuary*. Beijing: M] Science Press.

Jia, Y., Wang, Z., and Liu, X. (2017). Research progress on field investigation and *in-situ* observation methods of submarine landslide [J]. *J. Ocean Univ. China (natural Sci. Ed.* 47 (10), 61–72.

Lai, X., and Ye, Y. (2011). *Study on submarine landslide types and sliding mechanism in tidal channel area off the coast of eastern Zhejiang [C].China Offshore Engineering Symposium*.

Lai, X., Ye, Y., and Xie, Q. C. (2000). Types and characteristics of underwater landslides in tidal channel area of eastern Zhejiang [J]. *Donghai Ocean.* 18 (004), 1–8.

Liam Finn, W. D., Siddharthan, R., and Martin, G. R. (1983). Response of seafloor to ocean waves. *J. Geotech. Engrg.* 109 (4), 556–572. doi:10.1061/(asce)0733-9410(1983)109:4(556)

Liu, B., Nian, T., Liu, M., Zheng, D., song, L., and Yin, P. (2016). Stability evaluation of submarine slope based on upper bound method of limit analysis [J]. *Acta Oceanogr. Sin.* 38 (7), 135–143.

Liu, X., Jia, Y., and Zheng, J. (2015). Field experimental study on excess pore pressure response of seabed sediments in the Yellow River Estuary caused by waves [J]. *Geotech. Mech.* 36 (11), 3055–3062.

Liu, X. L., Jia, Y. G., Zheng, J. W., Hou, W., Zhang, L., Zhang, L. P., et al. (2013). Experimental evidence of wave-induced inhomogeneity in the strength of silty seabed sediments: Y ellow River delta, China. *Ocean. Eng.* 59, 120–128. doi:10.1016/j.oceaneng.2012.12.003

Liu, X., Lu, Y., and Wang, Y. (2020). Exploration of marine resources and marine engineering geology:Summary on the 2nd international symposium on marine engineering geology[J]. *J. Eng. Geol.* 28 (1), 169–177. doi:10.13544/j.cnki.jeg.2019-493

Liu, Y., Xia, X., and Jia, J. (2007). Sediment dynamics and erosion and deposition evolution characteristics of the coastal slope of Zhoushan waidiaoshan [J]. *Ocean. Bull.* (06), 53–60.

Liang, T., Xue, L., Hou, Y., Zhang, H., and Shan, H. (2021). Research on deformation of submarine slope in Zhoushan Islands by *in-situ* observation. *E3S Web Conf.* 261, 03015. doi:10.1051/e3sconf/202126103015

Nian, T., Liu, M., Liu, B., Zheng, D., song, L., and Yin, P. (2016). Analysis of seabed stability of clayey slope under extreme wave conditions [J]. *Ocean. Eng.* 34 (4), 9–15.

Prior, D. B., Suhayda, J. N., Lu, N. Z., Bornhold, B. D., Keller, G. H., Wiseman, W. J., et al. (1989). Storm wave reactivation of a submarine landslide. *Nature* 341 (6237), 47–50. doi:10.1038/341047a0

Rahman, M. S. (1997). Instability and movement of oceanfloor sediments: A review. *Int. J. Offshore Polar Eng.* 7 (3), 220–225.

Rahman, M. S., and Jabery, W. Y. (1986). A simplified drained analysis for wave-induced liquefaction in ocean floor sands. *Soils Found.* 26 (1), 57–68. doi:10.3208/sandf1972.26.3_57

Rahman, M. S. (1991). Wave-induced instability of seabed: Mechanism and conditions. *Mar. Geotechnol.* 10, 277–299. doi:10.1080/10641199109379896

Stegmann, S., Sultan, N., Garziglia, S., Pelleau, P., Appriroual, R., Kopf, A., et al. (2012). "A long-term monitoring array for landslide precursors: A case study at the ligurian slope (western mediterranean sea)," in *Offshore technology conference*.

Sultan, N., V oisset, M., Marsset, B., Marsset, T., Cauquil, E., and Colliat, J. L. (2007). Potential role of compressional structures in generating submarine slope failures in the Niger Delta. *Mar. Geol.* 237 (3), 169–190. doi:10.1016/j.margeo.2006.11.002

Uhlemann, S., Smith, A., Chambers, J., Dixon, N., Dijkstra, T., Haslam, E., et al. (2016). Assessment of ground-based monitoring techniques applied to landslide investigations. *Geomorphology* 253, 438–451. doi:10.1016/j.geomorph.2015.10.027

Urlaub, M., Petersen, F., Gross, F., Bonforte, A., Puglisi, G., Guglielmino, F., et al. (2018). Gravitational collapse of Mount Etna's southeastern flank. *Sci. Adv.* 4 (10), eaat9700. doi:10.1126/sciadv.aat9700

Vanneste, M., Sultan, N., Garziglia, S., Forsberg, C. F., and L'Heureux, J. S. (2014). Seafloor instabilities and sediment deformation processes: The need for integrated, multi-disciplinary investigations. *Mar. Geol.* 352, 183–214. doi:10.1016/j.margeo.2014.01.005

Wallace, L. M., Webb, S. C., Ito, Y., Mochizuki, K., Hino, R., Henrys, S., et al. (2016). Slow slip near the trench at the Hikurangi subduction zone, New Zealand. *Science* 352 (6286), 701–704. doi:10.1126/science.aaf2349

Wang, Hu (2015). *Mechanism and evaluation method of seabed instability in the Yellow River Delta under wave action [D]*. Qingdao: Ocean University of China.

Wang, Z., Jia, Y., Liu, X., Wang, D., Shan, H., Guo, L., et al. (2018). *In situ* observation of storm-wave-induced seabed deformation with a submarine landslide monitoring system. *Bull. Eng. Geol. Environ.* 77 (3), 1091–1102. doi:10.1007/s10064-017-1130-4

Wang, Z., Sun, Y., Jia, Y., Shan, Z., Shan, H., Zhang, S., et al. (2020). Wave-induced seafloor instabilities in the subaqueous Yellow River delta—Initiation and process of sediment failure. *Landslides* 17 (8), 1849–1862. doi:10.1007/s10346-020-01399-2

Wei, Y. (2015). *SAA measurement technology and its application in slope monitoring [D]*. Nanjing: Nanjing University.

Xu, G. (2006). *Study on submarine sliding of silty soil gentle slope caused by waves – Taking the underwater delta of the Yellow River as an example [D]*. Qingdao: Ocean University of China.

Xu, Q. (2020). Understanding the landslide monitoring and early warning: Consideration to practical issues[J]. *J. Eng. Geol.* 28 (2), 360–374. doi:10.13544/j.cnki.jeg.2020-025

Xue, L., Jia, Y., Hou, Y., Liang, T., Shan, H., Shan, Z., et al. (2020). Stability of submarine landslides by *in situ* observation. *IOP Conf. Ser. Earth Environ. Sci.* 570, 062038. doi:10.1088/1755-1315/570/6/062038

Yang, Z., and Chen, W. (1994). Subaqueous landslide system of the Yellow River [J]. *Ocean Limnol.* 25 (6), 573–581.

Zhang, C. (2013). *Study on tidal current and sediment characteristics in the offshore area of Zhujiajian Island [D]*. Shanghai: East China Normal University.

Zhang, M., Huang, Y., and Bao, Y. (2016). The mechanism of shallow submarine landslides triggered by storm surge. *Nat. Hazards (Dordr).* 81 (2), 1373–1383. doi:10.1007/s11069-015-2112-0

Zhang, S., Jia, Y., Wang, Z., Wen, M., Lu, F., Zhang, Y., et al. (2018a). Wave flume experiments on the contribution of seabed fluidization to sediment resuspension. *Acta Oceanol. Sin.* 37 (3), 80–87. doi:10.1007/s13131-018-1143-2